


RESEARCH ARTICLE OPEN ACCESS

Enzyme-Responsive Porous Scaffolds by Electrospinning Polyalanine

 Patrick A. Wall¹ | Charles Brooker² | Giuseppe Tronci^{2,3}  | Paul D. Thornton² 
¹School of Chemistry, University of Leeds, Leeds, United Kingdom | ²Leeds Institute of Textiles and Colour (LITAC), School of Design, University of Leeds, Leeds, United Kingdom | ³School of Dentistry, St. James's University Hospital, University of Leeds, Leeds, United Kingdom

Correspondence: Paul D. Thornton (p.d.thornton@leeds.ac.uk)

Received: 27 August 2025 | **Revised:** 18 November 2025 | **Accepted:** 19 November 2025

Keywords: electrospinning | enzyme-responsive materials | poly(amino acids) | porous materials | ring-opening polymerization

ABSTRACT

Porous polymeric materials are essential for applications ranging from tissue regeneration to controlled drug delivery, with a growing demand for them to be biodegradable and synthesized via environmentally responsible methods. In this work, we present a novel approach that addresses these needs by first synthesizing polyalanine (PAla) through a green and cost-effective ring-opening polymerization of its 2,5-diketopiperazine monomer. The resulting PAla was then co-electrospun with poly(ϵ -caprolactone) (PCL) to create robust, nanofibrous scaffolds. The inclusion of PAla resulted in a 399% increase in the material's maximum tensile stress compared to PCL alone, creating a tough material suitable for mechanically demanding applications. Crucially, these scaffolds demonstrated 'smart' behavior, exhibiting selective degradation in the presence of human neutrophil elastase (HNE), an enzyme overexpressed in chronic wounds. This work pioneers the creation of mechanically competent, enzyme-responsive biomaterials from a sustainable poly(amino acid) source, presenting a significant advance for potential PCL applications.

1 | Introduction

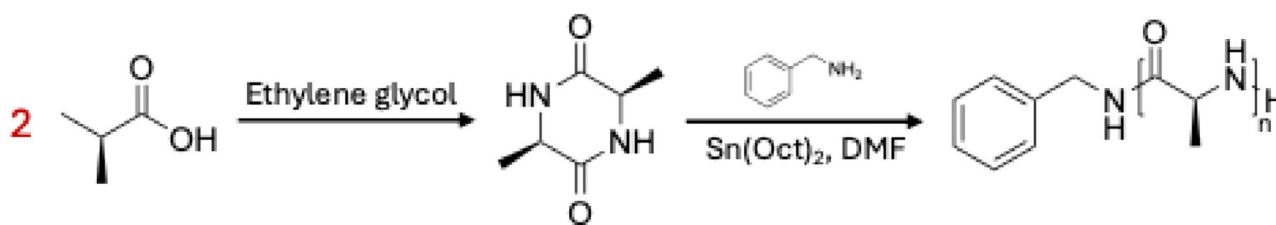
Porous polymeric materials are 3D structures that contain voids, or pores, throughout the material [1]. The versatility to produce polymeric scaffolds of different chemical functionalities and mechanical properties by simple changes to the polymer synthesis and/or processing ensures their wide-ranging applicability. Successful material uses include matrices for controlled drug delivery [2], scaffolds for 3D cell culture and tissue engineering [3], catalytic supports [4], chemical and biological sensors [5], and implants [6]. Although polymer scaffolds designed for use in catalysis and filtration are commonly produced from environmentally persistent, non-biodegradable polymers, applications that involve in vivo implementation of the porous material, such as scaffolds for tissue engineering and chronic wound healing devices, often require material degradability to eliminate the

need for their removal post-deployment. Consequently, there is a necessity for the creation of highly functional and tuneable biodegradable polymers that can be processed to form porous polymeric materials, particularly for use within the context of healthcare technologies.

Numerous methods to create porous polymeric materials exist, including emulsion templating [7], particle leaching [8], gas foaming [9], and 3D printing [10]. In addition, the electrospinning of polymer dissolved in an appropriate solvent enables the production of nanofibers with high surface area [11]. Polymeric scaffolds may be formed with consistent and controllable porosity and constant fiber diameters. Electrospinning is energy-efficient and results in complete conversion of polymer to the desired material when performed under optimized conditions. The process is tolerant to a wide range of polymers and is straightforward

This is an open access article under the terms of the [Creative Commons Attribution](https://creativecommons.org/licenses/by/4.0/) License, which permits use, distribution and reproduction in any medium, provided the original work is properly cited.

© 2025 The Author(s). *Macromolecular Chemistry and Physics* published by Wiley-VCH GmbH



SCHEME 1 | The facile synthesis of Ala DKP.

TABLE 1 | The parameters used for electrospinning PCL and PCL/PAla nanofibers, including solvent selection, weight percentage of polymer in solution, ratio of polymer solutions, potential difference applied during electrospinning, flow rate of solution, and time of electrospinning.

| Spin | Polymer 1 | Solvent (wt.% of polymer) | Polymer 2 | Solvent (wt.% of polymer) | Ratio of Polymer Solutions | Potential difference (kV) | Flow rate (mL/h) | Time (h) |
|------|-----------|-----------------------------|-----------|-----------------------------|----------------------------|---------------------------|------------------|----------|
| 1 | PCL | HFIP (7%) | — | — | — | 11 | 1 | 1 |
| 2 | PCL | HFIP/CHCl ₃ (7%) | — | — | — | 20 | 1.5 | 1 |
| 3 | PCL | HFIP/CHCl ₃ (7%) | PAla | DMF/ACN (5%) | 01:01 | 19 | 2 | 0.5 |
| 4 | PCL | HFIP/CHCl ₃ (7%) | PAla | DMF/ACN (5%) | 04:01 | 19 | 2 | 0.5 |
| 5 | PCL | HFIP (7%) | PAla | HFIP/CHCl ₃ (5%) | 01:01 | 11 | 2 | 0.75 |
| 6 | PCL | HFIP (7%) | PAla | HFIP/CHCl ₃ (5%) | 01:01 | 11 | 1 | 1 |
| 7 | PCL | HFIP (7%) | PAla | HFIP/CHCl ₃ (5%) | 01:01 | 20 | 2 | 1 |

to perform, making its employment to create advanced porous polymeric materials very attractive [12].

PCL is an excellent candidate for the creation of fibrous polymeric materials that may act as scaffolds for cell growth, and subsequent tissue regeneration or chronic wound repair. PCL is biodegradable and biocompatible, can be electrospun to create fibrous networks in a consistent manner, and is a cost-effective polymer [13]. However, PCL fibers lack inherent material strength and the capability for water uptake and retention. Consequently, PCL acts as an extremely effective base polymer for electrospinning, but it must be co-spun with polymers that offer mechanical strength to create durable porous materials. Polymers that enhance the properties of PCL were therefore sought, with poly(amino acids) identified as polymers that can offer material strength, without compromising polymer biodegradability, or environmentally-positive credentials.

Poly(amino acids) are exceptional polymers in that they are produced from a bio-renewable source (amino acids) and are biodegradable [14]. They also boast an extensive range of potential functionalities that are often not found in other bio-renewable and/or biodegradable polymers. Polymers with amino, carboxyl, hydroxyl, and thiol functionalities may be created from natural amino acids, depending on the amino acid polymerized [15, 16]. The functionalities that may be conferred by non-natural amino acids further expand on this to include alkene and

alkyne groups, amongst others [17]. The capability of poly(amino acids) to form secondary structures as a result of the hydrogen bonds that physically connect the polymer chains is a further key feature, enabling poly(amino acids) to form very stable structures ideal for controlled drug delivery applications [18], and mechanically strong materials. For instance, the PAla-rich segments found in spider silk are responsible for its remarkable strength, making PAla an ideal candidate for reinforcing biomaterials [19].

A major drawback of poly(amino acids) is the environmental and economic cost of their synthesis. Commonly, poly(amino acids) are created from N-carboxyanhydride (NCA) monomers, which are often, but not exclusively, created by the phosgenation of amino acid starting materials. In this reaction, triphosgene is commonly used in a reaction that is conducted in an organic solvent. The use of a lethal reactant and organic solvents in NCA creation renders the process environmentally detrimental and commercially implausible for many applications. Recently, we have demonstrated the use of 2,5-diketopiperazines (DKPs) formed from amino acids as alternative monomers for the creation of PAla and polyglycine [20]. DKPs may be created by the direct condensation of two amino acids in the absence of cyclization agents such as triphosgene. DKP ROP proceeds without atom loss, which contrasts with NCA ROP in which a molecule of carbon dioxide is lost for each NCA ring-opening. It may therefore be claimed that DKP ROP is safer and economically

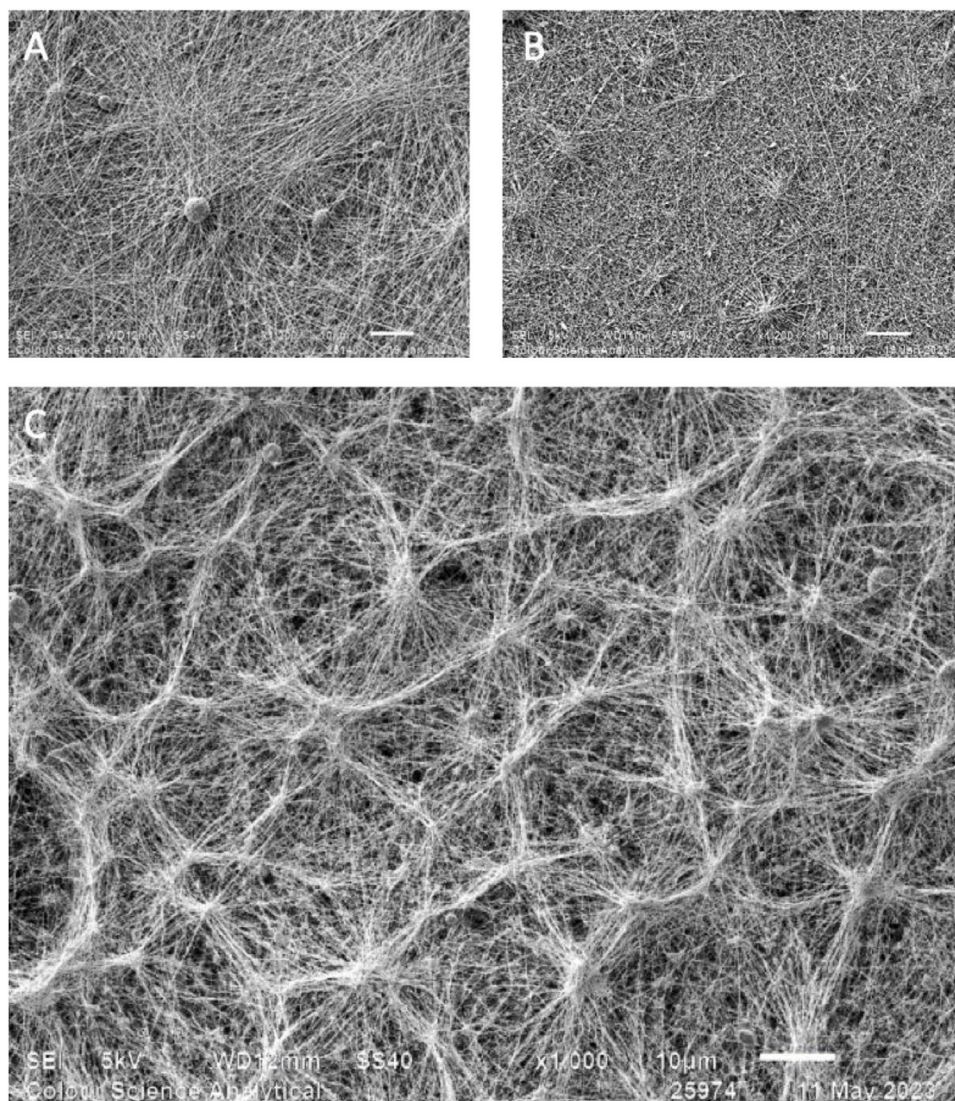


FIGURE 1 | Representative SEM images of PCL/PAla nanofibers produced in (A) spin 5, (B) spin 6, and (C) spin 7. Scale bars represent 10 μm in all images.

TABLE 2 | The masses of nanofiber samples before and after immersion in deionized water, their % water uptake, and mechanical testing results, including the maximum stress and strain, elastic moduli, and toughness of PCL and PCL/PAla nanofiber samples taken from spin 2 and spin 7, respectively. Toughness was calculated by integrating the stress–strain curve.

| Sample | Weight (mg) | | % Water Uptake | Maximum strain % | Maximum stress (MPa) | Elastic moduli (MPa) | | | Toughness ($\text{MJ}\cdot\text{m}^{-3}$) |
|----------|-------------|-------|----------------|------------------|----------------------|----------------------|----------------|---------------|---|
| | Before | After | | | | Initial, E | Tangent, E_t | Secant, E_s | |
| PCL | 0.5 | 1.7 | 240 | 93.1 | 2.46 | 3.13 | 2.01 | 2.64 | 2.14 |
| PCL/PAla | 2.8 | 19.5 | 596 | 59.1 | 12.28 | 36.58 | 26.00 | 20.78 | 3.59 |

advantageous compared to NCA ROP to produce PAla and polyglycine.

Electrospun polymeric materials offer advantageous properties suited to numerous applications. Such materials may support cell growth and proliferation if they boast appropriate biocompatibility and mechanical properties [21]. Polymer biodegradability

enables their in vivo use without invasive removal post-use, rendering them appropriate for application in tissue engineering and chronic wound healing applications [22]. The biocompatibility and biodegradability of poly(amino acids) render them appropriate for this application, but poly(amino acid) synthesis must be conducted in a cost-effective and responsible manner.

TABLE 3 | % mass loss, % beading, average fiber diameter, average pore diameter, and carbonyl intensities in FTIR spectra of PCL/PAla nanofiber samples that had been incubated with neutrophil elastase for 0, 0.5, 1, 1.5, and 2 h.

| Time (hrs) | % mass loss | % beading | Av. Fiber Diameter (nm) | σ | Av. Pore Diameter (nm) | σ | FTIR Carbonyl Intensity | | |
|------------|-------------|-----------|-------------------------|----------|------------------------|----------|-------------------------|------|-------|
| | | | | | | | PAla | PCL | Ratio |
| 0 | 0 | 0 | 120 | 41 | 249 | 83 | 61.2 | 24.2 | 2.5 |
| 0.5 | 5.8 | 2.2 | 76 | 18 | 393 | 143 | 54.8 | 39.5 | 1.4 |
| 1 | 15.9 | 1.5 | 61 | 13 | 393 | 167 | 52.7 | 47.5 | 1.1 |
| 1.5 | 24.6 | 4.4 | 52 | 14 | 597 | 338 | 38 | 58.9 | 0.6 |
| 2 | 35.5 | 3.6 | 49 | 13 | 1353 | 838 | 21.6 | 64.6 | 0.3 |

TABLE 4 | Maximum strain, maximum stress, elastic moduli, and toughness of PCL/PAla nanofiber samples that had been incubated with neutrophil elastase for 0, 0.5, 1, 1.5, and 2 h.

| Time (hrs) | Maximum strain % | Maximum stress (MPa) | Elastic Moduli (MPa) | | | Toughness (MJ·m ⁻³) |
|------------|------------------|----------------------|----------------------|-------------------------|------------------------|---------------------------------|
| | | | Initial, E | Tangent, E _T | Secant, E _S | |
| 0 | 59.1 | 12.28 | 36.58 | 26.00 | 20.78 | 3.59 |
| 0.5 | 62.6 | 11.55 | 10.96 | 26.72 | 18.44 | 2.91 |
| 1 | 65.1 | 9.78 | 15.96 | 14.28 | 15.03 | 3.32 |
| 1.5 | 67.6 | 7.201 | 16.77 | 14.64 | 10.66 | 2.11 |
| 2 | 69 | 6.55 | 9.47 | 9.66 | 9.49 | 1.14 |

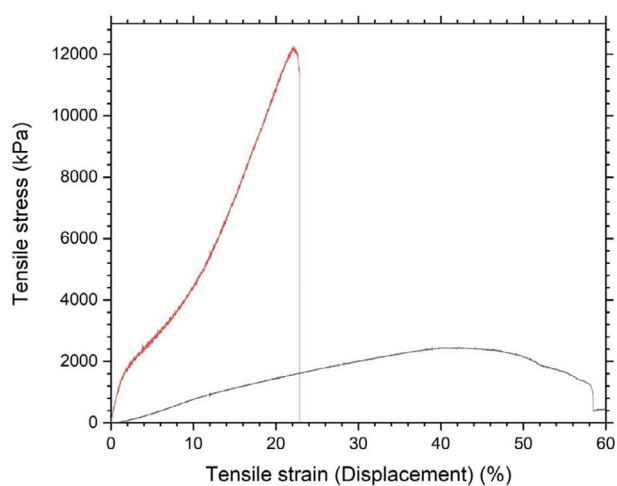


FIGURE 2 | Stress-strain curves of PCL nanofibers produced in spin 2 (black) and PCL/PAla nanofibers produced in spin 7 (red).

For applications in wound healing, the ability of a scaffold to manage moisture is paramount. An effective wound dressing must absorb excess exudate from the wound bed to prevent tissue maceration while simultaneously maintaining a moist environment that promotes cell migration and proliferation [23]. Therefore, a material's water uptake capacity is a critical parameter for evaluating its potential in regenerative medicine.

To address the critical need for mechanically competent and sustainable biomaterials, this study pioneers the creation of

a novel composite scaffold by co-electrospinning PAla with PCL. By leveraging a green and cost-effective ring-opening polymerization of its DKP monomer, we integrate a sustainably sourced PAla component to create hybrid fibers with transformative mechanical strength and superior water uptake compared to pure PCL. This work establishes a commercially plausible route to safer, high-performance biopolymers and unlocks the potential of PAla as a key functional component for engineering the next generation of advanced composite materials.

2 | Results and Discussion

PAla was synthesized via a two-step process. First, the monomer, alanine 2,5-diketopiperazine (Ala-DKP), was produced by the direct condensation of two L-alanine molecules (Scheme 1). DKP monomers are created in ethylene glycol in the absence of cyclization agents and are not reliant on a scavenger for hydrogen chloride, unlike NCA synthesis using triphosgene. DKP synthesis boasts simplicity, cost-effectiveness, and low environmental impact, with Ala-DKP synthesis achieved at 76.4% yield, which is comparable to yields obtained for Ala-NCA synthesis [24]. FTIR spectroscopy revealed the carbonyl bonds of the DKP lactam that forms (Figure S1), which was confirmed by ¹H NMR spectroscopy (Figure S2) and LC-MS analysis (Figure S3). This LC-MS spectrum confirms the successful synthesis of Ala-DKP by showing the characteristic protonated molecule at *m/z* 142.86 and its protonated dimer at *m/z* 284.88.

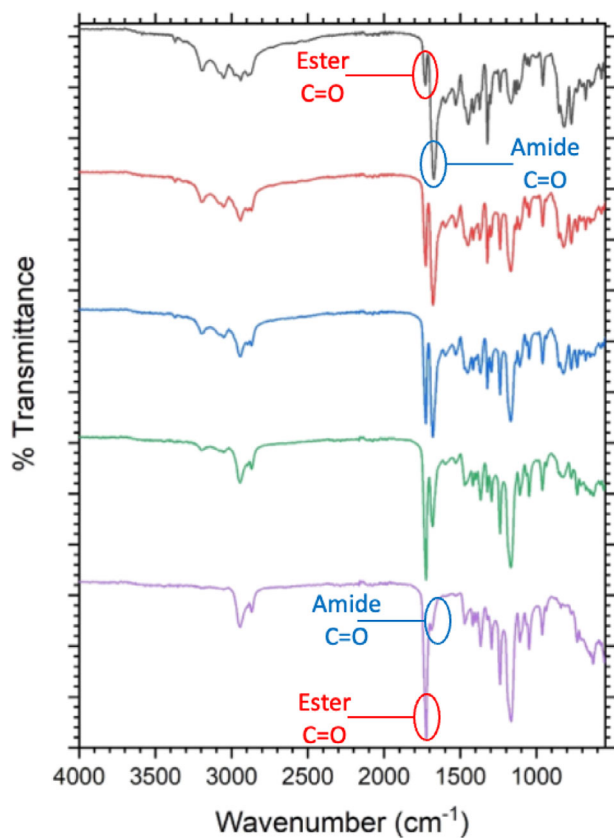


FIGURE 3 | FTIR spectra of PCL/PAla nanofiber samples produced in spin 7 before (black) and after incubation with neutrophil elastase for 30 min (red), 1 h (blue), 1.5 h (green), and 2 h (purple).

PAla was synthesized to provide strength to high molecular weight electrospun PCL fibers (PCL molecular weight = 70 g mol⁻¹). The electrospinning of PAla has been demonstrated previously [25], but we were unable to produce electrospun fibers of sufficient quality of mechanical properties from PAla on its own for the intended application. PCL is biocompatible and, most notably, it can be electrospun with relative ease. By combining PAla with PCL, fibers with enhanced mechanical properties and elastase responsiveness may be created. To create PAla, Ala DKP was dissolved with benzylamine (initiator) in anhydrous DMF and stirred at 130 °C under a constant flow of N_{2(g)} for 167 h, with stannous octoate used as the catalyst. The toxicity of stannous octoate is acknowledged, although stannous octoate was not detected by ¹H NMR spectroscopy in the PAla produced. FTIR spectroscopy did not provide substantial information concerning polymer synthesis owing to the similarities in chemical structures of the cyclic peptide monomer and peptide product (Figure S4). ¹H NMR spectroscopy revealed the five phenyl protons which come to resonance between 7.14 and 7.26 ppm were normalized against peaks representative of PAla at 1.26 ppm (CH₃), 3.84–3.93 ppm (CH), 8.08 ppm (NH of the amide bond formed), revealing 65 Ala repeat units on average in the PAla produced (Figure S5). Analysis by MALDI-TOF mass spectrometry (Figure S6) gave a distribution with M_n = 4,900 g mol⁻¹ and M_w = 5,300 g mol⁻¹, signifying 71 repeat units, 89% monomer conversion, and a narrow Đ of 1.07.

The optimum parameters for electrospinning PAla with a PCL carrier to produce nanofibers with an average fiber diameter between 50 and 500 nm were then sought. Fibers of these dimensions closely mimic the natural scale of the body's extracellular matrix, providing an ideal scaffold that encourages skin cells to attach, grow, and repair the wound. A variety of parameters were trialed (Table 1) and the resultant nanofibers assessed by SEM, to obtain a population distribution of nanofiber and pore diameters (Figures S7–S9), and FTIR spectroscopy to confirm the presence of key functional groups (Figures S10–S16).

Initially, PCL was dissolved in hexafluoroisopropanol (HFIP) at a concentration of 7 wt.% and electrospun with a potential difference of 11 kV and a flow rate of 1 mL/h. Analysis by SEM (Figure S7-A) showed a distribution of nanofiber diameters with an average width of 71 nm (SD = 24 nm, n >50) and 10.5% of beading/electrospray by area. Despite somewhat successful fiber formation, the substantial amount of beading and electrospray, as well as a relatively small fiber diameter, were non-ideal for the intended use. The occurrence of electrospray indicates low viscosity and low potential difference. Beading within nanofibers may result in a drug delivery material that enables prolonged release of any therapeutics from the scaffold [26], but it can compromise the physical properties of the network, detrimentally affecting the applicability of the material as a wound healing dressing. As such, the subsequent attempt at producing PCL nanofibers (Table 1, Spin 2) utilized a solution of PCL dissolved in 1:1 HFIP/chloroform at 7 wt.%, with the electrospinning done at an increased flow rate of 1.5 mL/h to increase average nanofiber diameter, and an increased potential difference of 20 kV to reduce beading and electrospray. Analysis of spin 2 by SEM (Figure S7-B) showed a larger average nanofiber diameter of 315 nm (SD = 187 nm) and no beading/electrospray. As such, these parameters were taken as an improvement upon spin 1.

To electrospin PCL/PAla nanofibers, PCL was dissolved as described for spin 2, and PAla was added to a 1:1 ratio of DMF/ACN at 5wt.%. The two solutions were combined in a 1:1 ratio and electrospun at a flow rate of 2 mL/h and a potential difference of 19 kV (Table 1, Spin 3). Analysis by SEM (Figure S8-A) revealed nanofibers with an average diameter of 75 nm (SD = 25 nm) with more beading and electrospray than fiber content. This may have resulted from the slow evaporation rate of the DMF/ACN solvent mixture or limited PAla solubility in the DMF/ACN solvent mixture. A repeat of spin 3 with a higher ratio of PCL solution to PAla solution (4:1) (Table 1, Spin 4) showed similar amounts of electrospray and beading (Figure S8-B). As such, an alternative solvent system for PAla was trialed.

Complete polymer solubility is essential for controlled electrospinning. HFIP was selected as a particularly suitable solvent owing to its capability to dissolve polymers that form extensive hydrogen bond networks, such as PAla. For spin 5, PCL was dissolved in HFIP at a concentration of 7 wt.%, and PAla was dissolved in a 1:1 ratio of HFIP/chloroform at a concentration of 5wt.%. The two solutions were combined in a 1:1 ratio and electrospun with a potential difference of 11 kV and a flow rate of 2 mL/h. Analysis by SEM (Figure S9-A) showed a marked reduction in electrospray and beading, with an average nanofiber diameter of 60 nm (SD = 17 nm). Spin 5 was repeated (Table 1, Spin 6) with half the flow rate (1 mL/h) and showed even less

electrospray and beading (Figure S9-B), with a similar average nanofiber diameter of 62 nm (SD = 15 nm). To increase the average nanofiber diameter, spin 5 was repeated again (Table 1, Spin 7) with an increased potential difference of 20 kV. Analysis of the resultant nanofiber mat by SEM (Figure 1) showed very little electrospray or bead formation, with an average nanofiber diameter of 120 nm (SD = 41 nm). The conditions used in spin 7 were taken as the most optimum due to the morphology of the resultant nanofiber mat. These optimized parameters successfully balanced solvent evaporation and charge density, yielding uniform fibers that were ideal for subsequent mechanical and material development. It may be hypothesized that the higher voltage in the HFIP/chloroform solvent system specifically helped to overcome surface tension and prevent beading without causing the electrospray seen in other attempts. This is significant as PAIa may offer enhanced strength to such networks, and may be hydrolyzed selectively by the protease elastase.

Porous PAIa-PCL materials have been created for the first time. Although the application of these materials should not be limited to use as scaffolds for tissue engineering, all the PCL/PAIa nanofiber mats produced had average nanofiber diameters within the range of fiber diameter that is most prevalent within natural ECM (50–500 nm) and were therefore suitable as a mimic of the physical structure of natural ECM. This demonstrates that the inclusion of PAIa successfully transforms the PCL-based mat from a relatively weak scaffold into a mechanically robust material suitable for applications where structural integrity is paramount. The average pore sizes of all PCL/PAIa mats were greater than 200 nm and less than 1 μ m. As such, all the mats had sufficient porosity for gas permeation [27], but narrow enough pores that they may prevent microbial infiltration and cell ingrowth, which may prevent infection and allow for removal of the material from a wound site without causing secondary wound damage [28].

To assess the potential application of these materials, a number of studies were undertaken. Initially, the capability of the scaffolds to absorb and maintain water was monitored. Effective wound dressings require the capacity to both maintain moisture levels and absorb exudate at a wound site [26]. As such, assessment of water uptake capacity (Table 2) by the nanofiber mats was conducted via weight measurements to determine their capacity to absorb and maintain water, providing evidence for their potential efficacy as wound dressings. The nanofiber mats from spin 2 and spin 7 were selected for water uptake assessment as they had the most consistent diameters of the PCL and PCL/PAIa nanofiber mats created. A portion of each was taken, weighed, and immersed in deionized water for 24 h. After which, the excess water was removed from the surface of the samples by patting dry using filter paper, and the samples were weighed again. The water uptake percentage results are reported in Table 2, and calculated as follows:

$$\text{Wateruptake \%} = \frac{\text{Massafter} - \text{Massbefore}}{\text{Massbefore}} \times 100$$

Despite the hydrophobicity of PCL, the PCL nanofiber mat produced from spin 2 had a water uptake percentage of 240%. This may be as a result of the capacity of PCL to act as a hydrogen bond acceptor, facilitating water binding. Whilst PAIa is also a hydrophobic polymer, it is less hydrophobic than PCL as a

consequence of its capacity to both accept and donate in hydrogen bonding, as well as the wicking effect due to the electrospun microstructure. The PCL/PAIa nanofiber mat produced in spin 7 had a water uptake percentage of 596%; a substantially higher percentage than that of PCL nanofibers alone. As such, the inclusion of PAIa in PCL nanofibers can dramatically improve water uptake, enhancing the material's applicability as dressings for high-exuding wounds, as well as those requiring a moist environment to be maintained.

The tensile properties of PCL and PCL/PAIa nanofiber mats produced in spins 2 and 7, respectively, were then assessed (Figure 2 and Table 2). Critically, the inclusion of PAIa transformed the mechanical landscape of the scaffold. While enhancing toughness by 68%, it dramatically amplified the ultimate tensile strength by an unprecedented 399% compared to PCL alone, converting a pliable base material into a robust, load-bearing network. Such increased toughness is important for the creation of engineered tissue that needs to withstand mechanical forces, such as in bone, cartilage, or tendon repair. The elasticity of the PCL/PAIa nanofiber mats was reduced compared to PCL, but their enhanced ultimate tensile strength renders them highly suited for chronic wound healing. The ultimate tensile strength of healthy human skin can be between 7.13 and 69.77 MPa, depending on the site of the skin on the body and the age of the donor [29]. The PCL/PAIa nanofiber mat boasted a maximum tensile strength well within the range of healthy human skin, further suggesting great potential for use as a wound healing dressing. Achieving mechanical properties within this physiological range is crucial; a dressing that is too stiff could cause stress and damage to the surrounding wound bed, while one that is too flimsy may fail to provide adequate protection. The engineered scaffold's properties therefore, represent an excellent balance for this application.

Biodegradability is a common goal for many polymeric materials. In particular, biodegradability is advantageous to biomaterials that are intended to spend limited time in the body, such as drug delivery vehicles and regenerative tissue scaffolds, including those that facilitate chronic wound healing. HNE, a protease overexpressed in chronic wounds and impairs wound healing, is reported to cleave peptide bonds between small amino acids, such as alanine, and hydrolyze key protein components of the ECM, including elastin. HNE is therefore of relevance to this research and may cause the degradation of the PAIa-containing networks, providing a route to biodegradability for these materials irrespective of their application. We therefore hypothesized that HNE would selectively cleave the amide bonds of the PAIa component while leaving the ester-based PCL backbone intact, leading to controlled and predictable changes in the material's mass and structure.

Consequently, the PCL/PAIa nanofiber mats produced in spin 7 were assessed for sensitivity to HNE hydrolysis and material degradation. The PCL/PAIa nanofiber samples were incubated with 8U of HNE in deionized water at room temperature for 2 h. Samples were taken every half an hour during the study and assessed for changes in weight loss (Table 3) and material morphology via SEM analysis (Figure 4). While 2 h may appear rapid for degradation to occur, it should be pointed out that this is a proof-of-concept study and that in vivo degradation

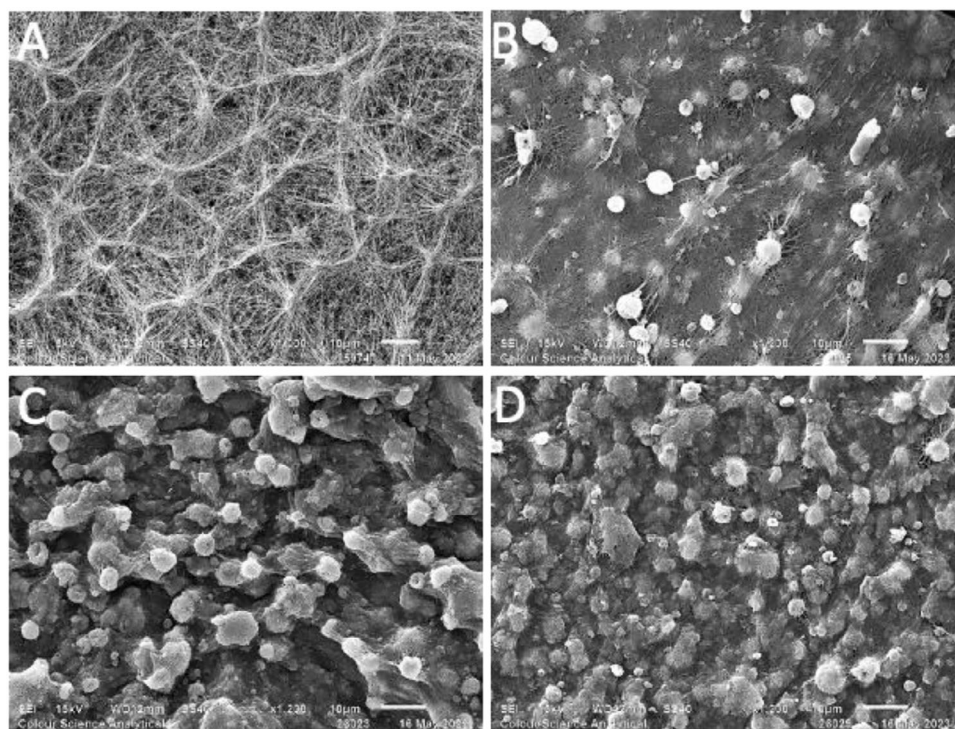


FIGURE 4 | SEM images of PCL/Pala nanofibers produced in spin 7 (A) 0 min, (B) 30 min, (C) 90 min, and (D) 120 min of incubation with 8U HNE.

rates are expected to be slower due to significantly lower HNE concentrations present at the chronic wound site [30].

Changes in the molecular composition of the polymeric fibers upon exposure could also be detected by FTIR spectroscopy (Figure 3 and Table 3). Specifically, the carbonyl peak of the amide bond (1674 cm^{-1}) that links the alanine repeat units of Pala is distinct from the carbonyl peak of the ester bond (1725 cm^{-1}) that links PCL repeat units. HNE-mediated degradation resulted in the cleavage of the amide bonds, reducing the intensity of the associated peak. This is reflected in Table 3 by comparing the ratio of intensities of the amide to ester carbonyl peaks, which decreases from 2.5 (0 h) to approaching zero after 2 h. Figure 3 shows that the amide carbonyl peak is significantly more pronounced prior to elastase addition, but over time, peak intensity favors the ester peak from 1 h onward. Although some amide peaks remain at 2 h, the peak is no longer sharp or distinct, indicating that extensive amide hydrolysis has occurred. This result emphasizes the selectivity that HNE has to preferentially cleave the amide bonds that link Ala repeat units over hydrolyzing PCL. The hydrolysis of Pala chains, as suggested by FTIR spectroscopic analysis, was supported by a reduction in the nanofiber mat mass over time for materials incubated with HNE (Table 3). A mass loss of more than 35% was reported after 2 h HNE incubation compared to the absence of mass loss found for materials stored in the absence of HNE (DI water only). Degradation of PCL in the control experiment, in which PCL fibers were subjected to HNE was not detected by FTIR (Figure S17) or SEM (Figure S18) analysis.

Analysis of the incubated PCL/Pala nanofiber samples by SEM showed that with increased incubation time in the HNE-rich

medium, average fiber diameter decreased from 120 to 49 nm (Table 3). Additionally, increased incubation with HNE showed an increase in average pore diameter from 249 to 1353 nm. Beyond these quantitative changes, the SEM images in Figure 4 reveal a dramatic morphological transformation. The well-defined fibrous network present at the start of the study appears to coalesce during enzyme exposure, resulting in a more continuous, fused surface after 120 min, which visually confirms the loss of structural Pala. Despite this, the nanofiber mat remained intact, with the matrix maintained after 2 h of exposure to HNE. These observations further support selective Pala degradation, with the PCL backbone remaining intact. This highly selective, enzyme-triggered degradation establishes these scaffolds as a ‘smart’ biomaterial. The ability to dynamically alter the material’s porosity in direct response to a disease-relevant enzyme (HNE) represents a key advance for engineering on-demand, porous controlled-release systems. This degradation-induced increase in pore size from an initial state that prevents cell infiltration to a final state that could permit it highlights a pathway for designing scaffolds that evolve with the healing process [31].

The tensile properties of the nanofibers that had undergone incubation with HNE were then assessed (Table 4 and Figure 5). As anticipated, a reduction in the maximum material stress (from 12.28 to 6.55 MPa) and toughness (3.59 to 1.14 MJ.m^{-3}) accompanied the hydrolysis of Pala chains by HNE. The cleavage of H-bonding Pala chains also corresponded to increased maximum strain values and reduced elastic moduli, corresponding to reduced physical crosslink density due to Pala cleavage. Even at the relatively low molecular weight of the Pala used, its impact on the porous material’s mechanical properties is explicit, suggesting

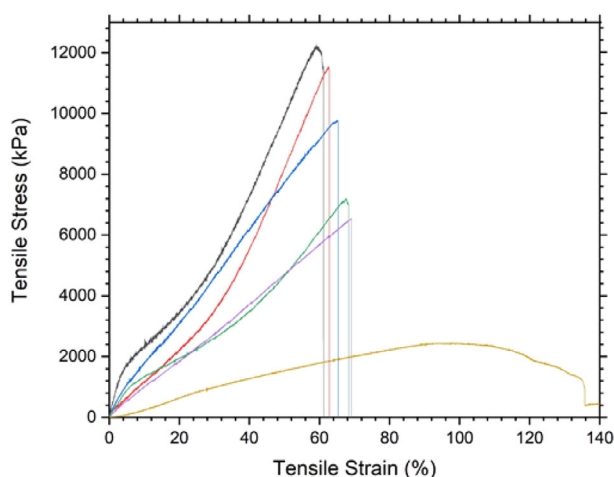


FIGURE 5 | Stress-strain curves of PCL nanofibers (brown), PCL/PAla nanofibers before (black) and after incubation with elastase for 30 min (red), 1 h (blue), 1.5 h (green), and 2 h (purple).

that the mechanical properties of such materials can be widely varied in a straightforward manner that is simply dependent on the PAla content.

3 | Conclusions

In this work, we have successfully translated a green polymer synthesis into a functional, enzyme-responsive biomaterial, in which the PAla component is selectively degraded, by electrospinning PAla with PCL for the first time. PAla was produced in an environmentally positive manner, via the ring-opening polymerization of its DKP. The extensive capability of PAla to form an extensive array of hydrogen bonds between polymer chains enables its use to add mechanical strength to porous materials. We demonstrate that PAla can positively impact the maximum tensile strength of PCL fibers, enabling the creation of durable nanofiber mats for potential use as scaffolds for tissue regeneration. The PAla component of the nanofiber mats is degradable upon interaction with HNE, ensuring that the polymer implant is non-permanent and suitable for potential application to aid chronic wound healing; the porous material is envisaged to aid cell proliferation, skin regrowth, before polymer degradation occurs in response to overexpressed HNE. Future work will focus on leveraging these tunable properties by loading these scaffolds with therapeutic agents and assessing their cytocompatibility and regenerative potential in in vitro models of wound healing.

Conflicts of Interest

The authors declare no conflicts of interest.

Data Availability Statement

The data that support the findings of this study are available from the corresponding author upon reasonable request.

References

1. Q. Liu J. Xiong W. Lin, et al., "Porous Polymers: Structure, Fabrication and Application," *Materials Horizons* 12 (2025): 2436–2466.
2. Y. Tang A. Varyambath Y. Ding, et al., "Porous Organic Polymers for Drug Delivery: Hierarchical Pore Structures, Variable Morphologies, and Biological Properties," *Biomaterials Science* 10 (2022): 5369–5390, <https://doi.org/10.1039/D2BM00719C>.
3. F. J. V. P. Maksoud, M. F. Hann, A. J. Thanarak, et al., "Porous Biomaterials for Tissue Engineering: A Review," *Journal of Materials Chemistry B* 10 (2022): 8111–8165, <https://doi.org/10.1039/D1TB02628C>.
4. R. Poupat, D. Grande, B. Carbonnier, and B. Le Droumaguet, "Porous Polymers and Metallic Nanoparticles: A Hybrid Wedding as a Robust Method Toward Efficient Supported Catalytic Systems," *Progress in Polymer Science* 96 (2019): 21–42, <https://doi.org/10.1016/j.progpolymsci.2019.05.003>.
5. S. Wang, H. Li, H. Hunag, X. Cao, X. Chen, and D. Cao, "Porous Organic Polymers as a Platform for Sensing Applications," *Chemical Society Reviews* 51 (2022): 2031–2080, <https://doi.org/10.1039/D2CS00059H>.
6. R. S. Kovylin, D. Y. Aleynik, and I. L. Fedushkin, "Modern Porous Polymer Implants: Synthesis, Properties, and Application," *Polymer Science Series C* 63 (2021): 29–46, <https://doi.org/10.1134/S1811238221010033>.
7. T. Zhang, R. A. Sanguramath, S. Israel, and M. S. Silverstein, "Emulsion Templating: Porous Polymers and Beyond," *Macromolecules* 52 (2019): 5445–5479.
8. A. Prasad, M. R. Sankar, and V. Katiyar, "State of Art on Solvent Casting Particulate Leaching Method for Orthopedic Scaffolds Fabrication," *Materials Today: Proceedings* 4 (2017): 898–907.
9. M. Costantini and A. Barbetta, "Gas Foaming Technologies for 3D Scaffold Engineering," *Functional 3D tissue engineering scaffolds* (2018): 127–149.
10. C. Wang, W. Huang, Y. Zhou, L. He, Z. He, Z. Chen, X. He, S. Tian, J. Liao, Y. Wei, and M. Wang, "3D Printing of Bone Tissue Engineering Scaffolds," *Bioactive Materials* 5 (2020): 82–91, <https://doi.org/10.1016/j.bioactmat.2020.01.004>.
11. R. Liu, L. Hou, G. Yue, et al., "Progress of Fabrication and Applications of Electrospun Hierarchically Porous Nanofibers," *Advanced Fiber Materials* 4 (2022): 604–630.
12. A. Contreras M. J. Raxworthy S. Wood, and G. Tronci, "Hydrolytic Degradability, Cell Tolerance and On-Demand Antibacterial Effect of Electrospun Photodynamically Active Fibres," *Pharmaceutics* 12 (2020): 711, <https://doi.org/10.3390/pharmaceutics12080711>.
13. H. E. Owston K. M. Moisley G. Tronci S. J. Russell P. V. Giannoudis, and E. Jones, "Induced Periosteum-Mimicking Membrane with Cell Barrier and Multipotential Stromal Cell (MSC) Homing Functionalities," *International Journal of Molecular Sciences* 21 (2020): 5233, <https://doi.org/10.3390/ijms21155233>.
14. M. Khuphe and P. D. Thornton, *Engineering of Biomaterials for Drug Delivery Systems (Beyond Polyethylene Glycol)* (Wood Head Publishing Series in Biomaterials, 2018): 199–228.
15. M. Khuphe C. S. Mahon, and P. D. Thornton, "Glucose-Bearing Biodegradable Poly (Amino Acid) and Poly (Amino Acid)-Poly (Ester) Conjugates for Controlled Payload Release," *Biomaterials Science* 4 (2016): 1792–1801, <https://doi.org/10.1039/C6BM00535G>.
16. X. Jin and P. D. Thornton, "Thermal Deprotection: A Sustainable and Efficient Strategy for Synthesising α -polylysine Adsorbents," *RSC advances* (2025): 17397–17404.
17. J. Huang G. Habraken F. Audouin, and A. Heise, "Hydrolytically Stable Bioactive Synthetic Glycopeptide Homo- and Copolymers by Combination of NCA Polymerization and Click Reaction," *Macromolecules* 43 (2010): 6050–6057, <https://doi.org/10.1021/ma101096h>.

18. J. V. Rowley P. A. Wall H. Yu, et al., "Triggered and Monitored Drug Release From Bifunctional Hybrid Nanocomposites," *Polymer Chemistry* 13 (2022): 100–108, <https://doi.org/10.1039/D1PY01227D>.
19. A. Gitsas G. Floudas M. Mondeshki, et al., "Control of Peptide Secondary Structure and Dynamics in Poly(γ -Benzyl- L-Glutamate)-b-Polyalanine Peptides," *Macromolecules* 41 (2008): 8072–8080, <https://doi.org/10.1021/ma801770b>.
20. P. A. Wall C. O. H. Sajid K. Mitchinson, and P. D. Thornton, "Poly (Amino Acid) Synthesis from 2, 5-Diketopiperazines for Acid-Actuated Drug Release," *Macromolecular Materials and Engineering* 310 (2025): 2500091, <https://doi.org/10.1002/mame.202500091>.
21. S. Deshmukh M. Kathiresan, and M. A. Kulandainathan, "A Review on Biopolymer-Derived Electrospun Nanofibers for Biomedical and Antiviral Applications," *Biomaterials Science* 10 (2022): 4424–4442, <https://doi.org/10.1039/D2BM00820C>.
22. D. Veeman M. S. Sai P. Sureshkumar, et al., "Additive Manufacturing of Biopolymers for Tissue Engineering and Regenerative Medicine: An Overview, Potential Applications, Advancements, and Trends," *International Journal of Polymer Science* 2021 (2021): 4907027, <https://doi.org/10.1155/2021/4907027>.
23. I. Negut, G. Dorcioman, and V. Grumezescu, "Scaffolds for Wound Healing Applications," *Polymers* 12 (2020): 2010.
24. A. H. Morrell N. J. Warren, and P. D. Thornton, "The Production of Polysarcosine-Containing Nanoparticles by Ring-Opening Polymerization-Induced Self-Assembly," *Macromolecular Rapid Communications* 45 (2024): 2400103, <https://doi.org/10.1002/marc.202400103>.
25. K. Devarayan S. Nakagami S. Suzuki I. Yuki, and K. Ohkawa, "Electrospinning and Post-Spun Chain Conformations of Synthetic, Hydrophobic Poly(α -amino Acid)S," *Polymers* 12 (2020): 327.
26. M. Abrigo, S. L. McArthur, and P. Kingshott, "Electrospun Nanofibers as Dressings for Chronic Wound Care: Advances, Challenges and Future Prospects," *Macromolecular Bioscience* 14 (2014): 772–792, <https://doi.org/10.1002/mabi.201300561>.
27. S. Somvipart, S. Kanokpanont, R. Rangkupan, J. Ratanavaraporn, and S. Damrongsakkul, "Development of Electrospun Beaded Fibers from Thai Silk Fibroin and Gelatin for Controlled Release Application," *International Journal of Biological Macromolecules* 55 (2013): 176–184, <https://doi.org/10.1016/j.ijbiomac.2013.01.006>.
28. Y. Zhang, C. T. Lim, S. Ramakrishna, and Z.-M. Huang, "Recent Development of Polymer Nanofibers for Biomedical and Biotechnological Applications," *Journal of Materials Science: Materials in Medicine* 16 (2005): 933–946.
29. V. Holmdahl, O. Backman, U. Gunnarsson, and K. Strigård, "The Tensile Strength of Full-Thickness Skin: A Laboratory Study Prior to Its Use as Reinforcement in Parastomal Hernia Repair," *Frontiers in Surgery* 6 (2019): 69.
30. D. Kolahreez, L. Ghasemi-Mobarakeh, F. Quartinello, F. W. Liebner, G. M. Guebitz, and, D. Ribitsch, "Multifunctional Casein-Based Wound Dressing Capable of Monitoring and Moderating the Proteolytic Activity of Chronic Wounds," *Biomacromolecules* 25 (2024): 700–714, <https://doi.org/10.1021/acs.biomac.3c00910>.
31. A. T. Neffe B. F. Pierce G. Tronci, et al., "One Step Creation of Multifunctional 3D Architected Hydrogels Inducing Bone Regeneration," *Advanced Materials* 27 (2015): 1738–1744, <https://doi.org/10.1002/adma.201404787>.

Supporting Information

Additional supporting information can be found online in the Supporting Information section.

Supporting File: macp70163-sup-0001-SuppMat.docx